Methodology for Liquid Foam Templating of Hydrogel Foams: A Rheological and Tomographic Characterization

Manon Jouanlanne, Imene Ben-djemaa, Antoine Egelé, Leandro Jacomine, Jean Farago, Wiebke Drenckhan, Aurélie Hourlier-fargette

RESEARCH ARTICLE

Editor's Choice

ADVANCED MATERIALS INTERFACES Open Access

www.advmatinterfaces.de

Methodology for Liquid Foam Templating of Hydrogel Foams: A Rheological and Tomographic Characterization

Manon Jouanlanne, Imene Ben-Djemaa, Antoine Egelé, Leandro Jacomine, Jean Farago, Wiebke Drenckhan, and Aurélie Hourlier-Fargette**

Hydrogel foams are widely used in many applications such as biomaterials, cosmetics, foods, or agriculture. However, controlling precisely foam morphology (bubble size or shape, connectivity, wall and strut thicknesses, homogeneity) is required to optimize their properties. Therefore, a method is proposed here for generating, controlling, and characterizing the morphology of hydrogel foams from liquid foam templates: Using the example of Alginate-$CaHPO_4$-based hydrogel foams, a highly controllable foaming process is provided by bubbling nitrogen through nozzles into the solution, which produces hydrogel foams with millimeter-sized bubbles. A rheological characterization protocol of the foam's constituent material is first implemented and highlights the impact of the initial liquid foam properties and of the competition between the solidification kinetics and the foam aging mechanisms on the resulting morphology. X-ray tomographic characterization performed on solidifying and solidified samples then demonstrates that by controlling the temporal evolution of the foam via its formulation, it is possible to tune the final morphology of the alginate foams. This method can be adapted to other hydrogel or polymer formulations, foam characteristics and length scales, as soon as solidification processes happen on timescales shorter than foam destabilization mechanisms.

1. Introduction

Due to their interesting properties such as their biocompatibility, low density, large surface-to-volume ratio and rich mechanical properties, hydrogel foams are used in many different fields, from biomaterials, to cosmetics, foods, or agriculture.[1,2] Such hydrogel foams are generally disordered and polydisperse, but a higher level of control over the foam structure can be reached through a technique known as "liquid foam templating,"[3,4] consisting in tuning the morphology of a liquid precursor foam before solidification. This strategy requires the control of many parameters in terms of foam production: the foaming process, the initial viscosity of the used liquid, the solidification kinetics and the timescales of foam evolution (drainage, coarsening, coalescence, evaporation) which determine the foam morphology (bubble size or shape, connectivity, wall and strut thicknesses, homogeneity). To obtain solid foams with the same morphology as their liquid templates, the understanding of the different timescales involved in liquid foam templating is crucial: the bubbles need enough time after generation to reach mechanical equilibrium before solidification, but the solidification time needs to be short enough to avoid destabilization.

We focus here on the gelling of low-density hydrogel foams to obtain foam architectures that follow Plateau's laws: three films meet at 120° angles forming a liquid channel called a Plateau border (referred to as a strut when solidified), and four Plateau borders meet in a tetrahedral geometry.[5] To provide a general methodology for liquid foam templating of hydrogel foams, we combine here rheology and X-ray tomography to characterize and understand the temporal evolution of the system. Since bubble coalescence is efficiently suppressed by a surfactant, and gas exchange (coarsening) between the large monodisperse bubbles is very slow, we focus here on the influence of liquid drainage. Under the effect of gravity, the liquid (contained mainly inside the Plateau borders) flows from the top to the bottom of the foam. In the initial state, the foam is very dense and the Plateau borders are very thick, but as the foam drains they become thinner.[6] Thus, by controlling the solidification time, it is possible to stop the drainage and therefore solidify the foam at a given density.

It is therefore important to control the gelation kinetics: we require our formulations to remain in the liquid state to allow foaming before gelling begins, and then to gel rapidly to stop drainage and avoid foam destabilization. This corresponds to a delayed gelation mechanism. To do so, we consider a model hydrogel foam based on alginate and calcium phosphate dibasic salts ($CaHPO_4$). Alginates are polysaccharides extracted from brown seaweed algae (*Phaeophyceae*) and soil bacteria (*Azotobacter vinelandii*).[7] Gelation is instantaneous in the presence of Ca^{2+}

M. Jouanlanne, I. Ben-Djemaa, A. Egelé, L. Jacomine, J. Farago, W. Drenckhan, A. Hourlier-Fargette
Université de Strasbourg, CNRS, Institut Charles Sadron UPR22 Strasbourg F-67000, France
E-mail: mjouanlanne@unistra.fr; hourlierfargette@unistra.fr

The ORCID identification number(s) for the author(s) of this article can be found under https://doi.org/10.1002/admi.202400337

DOI: 10.1002/admi.202400337

ions, which is why direct external contact forms heterogeneous and poorly controllable gels, which is even more accentuated in the context of foam gelation, where diffusion of calcium to the center of the foam is difficult.[8] For these reasons, the most commonly used gelation method for making hydrogel foams is internal cross-linking.[7] In this method, Ca^{2+} ions are mixed with the alginate solution in an inactive form. In this work, we use Ca^{2+} in the form of solid salts ($CaHPO_4$), which are not soluble in water at basic pH but soluble at acidic pH to induce gelation.[9] The gelation is then initiated by the acidification of the Ca^{2+}-alginate solution. In most cases, including the work at hand, acidification is induced using Glucono-δ-lactone (GDL), which slowly decreases the pH through its hydrolysis to gluconic acid.[7]

The choice of this formulation allows to obtain a fast gelation which starts with a delay of ≈20 min after the addition of GDL, with an initial solution at a neutral pH, brought via the hydrolysis of Glucono-δ-lactone (GDL) to pH 4.[10] Another reason for working with this specific system lies in the mechanical properties of the obtained gels: Ben Djemaa et al.[10] showed that the formulations based on calcium salts which release the most Ca^{2+} result in the strongest gels and that the $CaHPO_4$ salt solution gives a particularly strong gel. This is interesting for foam fabrication to obtain free-standing samples that do not collapse under their own weight. We show here that Alginate-$CaHPO_4$-based formulations provide an excellent control over the gelation kinetics. In particular, we show that by controlling the GDL concentration, we can tune the initiation of gelation in a controlled manner and thus give enough time to the foam to drain while gelling before it destabilizes.

All the foams in this study were produced by bubbling gas through nozzles into a stationary foaming liquid. When a bubble forms at the nozzle, its buoyancy force is counterbalanced by surface tension forces and the bubble remains attached to the nozzle until its volume reaches a critical value. The bubble is then accelerated upward and detaches.[11,12] This method has already been studied experimentally[13–16] and theoretically[17] in order to obtain an adequate prediction of the bubble size. Many parameters can be used to control and adjust the bubble size to obtain customized foams: The gas pressure, the surface tension and the viscosity of the liquid, the dimensions and the shape of the nozzle, the wetting properties of the nozzle, the density of the gas and the liquid. These parameters control the regime in which bubbling occurs: quasi-static, viscous or inertial.[11,18] Contrary to the case of chemical foaming where bubbles are generated by chemical reactions, in the present work, the bubble size has been controlled for each bubble individually by physical bubbling.

Commonly produced alginate foams (regardless of the type of hydrogel or crosslinker, or the foaming technique) have pore sizes of less than 500 µm.[19] In this work, we produce monodisperse hydrogel foams with millimeter-sized bubbles (3–4 mm), as shown in **Figure 1**.

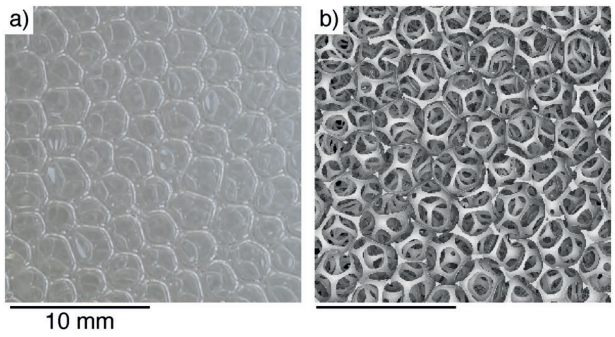

Figure 1. Alginate-$CaHPO_4$-based foam. a) Photograph and b) 3D reconstruction from X-ray tomographic images of foams with millimeter-sized bubbles (3–4 mm), produced following the protocol described in the Experimental Section. The samples presented here have been produced with a base solution of 1 wt% LVA and an added quantity of GDL of 3 wt%.

2. Experimental Section

2.1. Preparation of Solutions

To prepare alginate solutions, 2 wt% of alginic acid sodium salt, low viscosity alginate (LVA, purchased from Alfa Aesar) was solubilized in Milli-Q water under mechanical stirring at 50 °C for 30 min. The solution was kept under magnetic stirring and diluted to the desired concentrations (0.5–1 wt% of LVA, c_{LVA}) for the different experiments. To ensure reproducibility, this solution was used for 1 week maximum after preparation. To prepare the gelling solution, 0.02 M of calcium phosphate dibasic ($CaHPO_4$, purchased from Sigma–Aldrich) was dispersed into a 1 wt% solution of LVA using an IKA Ultra–Turrax disperser. This LVA/$CaHPO_4$ ratio was kept constant for all experiments. To this initial solution, 2 g of the surfactant Disponil APG 425 (from BASF) per 100 g of solution was added under gentle stirring to prevent the formation of bubbles for 5 min (the amount of surfactant was chosen to be well above the typical values of CMC of alkyl polyglucosides[20]). D-(+)-Gluconic acid δ-lactone (GDL, from Sigma–Aldrich) was finally added to the gelling solution to initiate the gelation by acidification. Different concentrations of GDL were considered, from 1 g per 100 g to 5 g per 100 g of the initial solution, denoted for simplicity as c_{GDL} = 1 to 5 wt% in the following. The GDL was first pre-dissolved in 1 g of water, subtracted from the total mass of water required, and then mixed with the rest for 30 s.

2.2. Rheological Characterization

Viscosity measurements: The viscosity μ_0 of the non-gelling LVA solutions (absence of $CaHPO_4$ and GDL) was measured using a DHR3 rheometer from TA Instruments at 20 °C with the cone-plate geometry (diameter of 60 mm, truncation gap of 28 µm, and angle of 1° 00 min 47 s), following the method of Andrieux et al.[21] The shear rates were varied from 0.1 to 1000 s^{-1}, with an acquisition time of ten points per decade. To avoid evaporation, the sample was covered using a "solvent trap and evaporation blocking" module filled with silicone oil (provided by TA Instruments). For each solution tested, the viscosity value taken as the zero-shear viscosity was obtained from fitting the Cross model to the data[22] (the obtained parameters of the Cross model are listed in Table S1, Supporting Information).

Gelation kinetics: The temporal evolution of the visco-elastic properties of LVA solutions undergoing gelation was measured using a HR20 rheometer from TA Instruments at 20 °C with the plate–plate geometry (diameter of 40 mm, sandblasted plate,

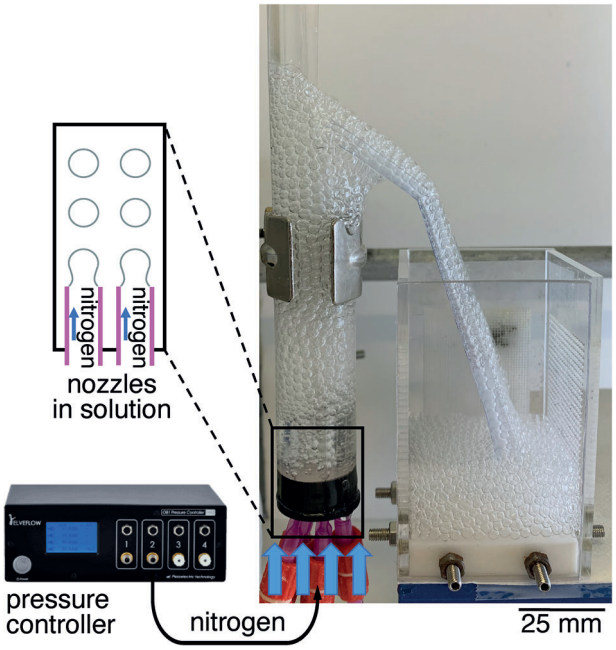

Figure 2. Experimental setup. Foam is generated by blowing nitrogen through four nozzles at constant pressure into an alginate solution (gelling or non-gelling). It flows down a ramp made of a PVC sheet, before entering in the collection container of square cross-section.

gap of 750 µm, frequency of 1 Hz, and amplitude of 2%). The solutions were prepared as explained in Section 2.1 but due to the small volume of solution required here, the mixing was carried out using a magnetic stirrer. The samples were placed in the rheometer with a pipette, ensuring the absence of bubbles, and the "solvent trap and evaporation blocking" module was placed above the sample. The gel time t_g was taken as the peak of the first derivative of the complex viscosity as a function of time, according to the definition of the gel time given by Winter and Chambon.[23]

2.3. Foam Generation

To obtain hydrogel foams with millimeter-sized bubbles, as illustrated in Figure 1, the experimental setup shown in **Figure 2** was used: the foam was first generated in a circular perspex tube (ID 25 mm), closed at the bottom. The plug closing the bottom of the tube was made of silicone elastomer (Zhermack Elite Double 22) to ensure a waterproof seal and to allow four nozzles (ID 150 µm) to pass through. Nitrogen was blown through the nozzles into 40 mL of the LVA solution (gelling or non-gelling) at a constant pressure (600 mbar) via an Elveflow pressure controller (OB1 MK3+) during 2 min. The foam then flowed from the circular tube to a 50 × 50 × 80 mm container via a connecting ramp made of a PVC sheet. Particular attention was paid to making the container watertight. The container was then filled to the brim with foam and covered with parafilm in contact with the foam. The resulting system makes it possible to study the drainage over time, with or without gelation of the foam. Moreover, correctly protected, the gelled foam was stable for a sufficient amount of time (almost 2 h) to be characterized via X-ray micro-tomography.

2.4. Foam Drainage Analysis

The foam formed in the square container was illuminated from the side by a diffusive, white light source. A video of the transparent wall of the container was recorded using a Canon EOS 77D camera, fitted with an EF 100 mm F/2.8 Canon macro objective lens. The obtained images (see Figure 6b for an example) show with visible contrast the foam in contact with the wall and the liquid draining out of the foam to its bottom. These images were first treated to increase brightness and contrast using the free ImageJ software.[24] Then, the evolution of drainage over time was monitored by measuring every minute the height h of the drained liquid at the bottom of the container (Figure 6b). Note that the initial height of all foams was identical, to allow a comparison between drainage heights of different samples.

2.5. X-Ray Microtomography Characterization

2.5.1. Imaging Process

The tomographic imaging was performed with an X-ray microtomograph EasyTom 150/160 from RX Solutions with a tube voltage of 90 kV and a power of 5.5 W. For all experiments, tomograms were launched 20 min after the foam fabrication, with a resolution of 25 µm covering a volume of ≈45 × 45 × 30 mm^3 located at the bottom of the foam (the bottom of the image starts at the boundary between the drained liquid and the foam). XAct software was used to generate stacks of image slices, which were then used to reconstruct 3D structures.

The phase segmentation of the images (i.e., the distinction between matter and gas) was initiated manually in the VG Studio MAX software to ensure that only the foam material was taken into account, using a cursor on a histogram evaluation.

The foam/powder analysis tool provided by the VG Studio software was used to measure several physical parameters at the bubble scale over the whole foam, such as the bubble size and the structure thickness (thickness of struts and vertices) of the entire sample.

To avoid errors in these measurements, two key points were important to control in the tomographic acquisition and in the VG Studio MAX software analysis: the resolution and the sensibility threshold for identifying bubbles and measuring their equivalent diameters. An adequate resolution was chosen as a function of the ratio between the source/sample and the source/detector lengths, as well as the size of the sample: at least three voxels were required across the thickness of an object. If this ratio is not respected, as is often the case for the thickness of the films separating two bubbles (smaller than the 25 µm resolution), the software would not be able to reconstruct those thin structures (Figures 1b and 3b). However, even if the films are not reconstructed, the software artificially creates edges to measure the bubble sizes. More precisely, in the use of the foam/powder analysis tool, a sensibility threshold was set to define the way the software artificially creates those missing boundaries between bubbles. With an inadequate threshold, the software would divide one bubble into multiple bubbles or merge multiple bubbles into

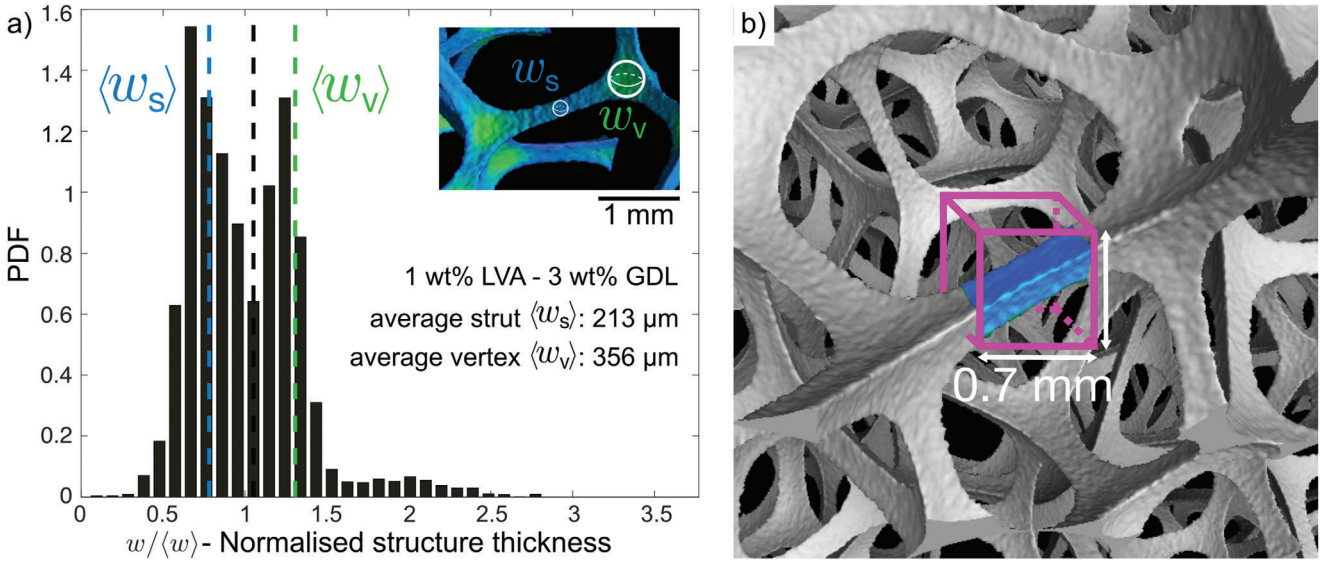

Figure 3. Structure thickness measurements. Example of the thicknesses measured on the tomographic images with the software VG Studio MAX, for an LVA foam produced following the protocol described in the Experimental Section, with c_{LVA} = 1 wt% and c_{GDL} = 3 wt%. a) PDF of the structure thicknesses used to measure strut and vertex thicknesses for a *Global Analysis*. The inset shows a zoom on a strut to explain the presence of two peaks corresponding to the thickness of the struts w_s (in blue on the image) and the vertices w_v (in green on the image). The black dashed line highlights the manual separation of these peaks. The blue dashed line shows the average thickness of the struts $\langle w_s \rangle$ and the green dashed line shows the average thickness of the vertices $\langle w_v \rangle$. b) Method used to measure strut thicknesses for a *Drainage Analysis at the scale of a strut*. Zoom on a randomly selected strut from a 3D reconstruction of an LVA foam. A 0.7 mm wide cubic region of interest is created to contain the strut.

one single bubble.[25] For this study, the threshold sensibility was kept at 20% after various tests.

2.5.2. Global Analysis

To measure the bubble size, the software uses the value of the equivalent diameter d, defined as the diameter of a sphere that has the same volume as the bubble. To determine the structure thickness w, the VG Studio software uses a surface determination and inscribes the largest fitting spheres inside the struts and vertices, measures their diameter, and provides a histogram showing the structure thickness distribution in the foam.

The Probability Density Function (PDF) of the structure thickness normalized by the mean structure thickness is then plotted, defined as the histogram of $w/\langle w \rangle$ where each bin count is divided by (N_{tot}*δn), where N_{tot} is the total number of counts and δn is the bin width. This definition ensures that a numerical integration gives always 1 whatever the choice of δn, such that the curves calculated were a bona fide approximation of the probability density function of $w/\langle w \rangle$ (Figure 3a).

On these PDFs, two peaks were clearly observed, corresponding to the thickness of 1) the struts w_s (left side of the black dashed line); and 2) the vertices w_v (right side of the black dashed line). The PDFs were manually separated in two at the local minimum between the two peaks to distinguish these two thicknesses. The black dashed line in Figure 3a highlights this separation. This differentiation between strut and vertex thicknesses had already been found in the literature, on images analyzed with the same VG Studio software.[26] The average thickness of the struts $\langle w_s \rangle$ was then calculated by taking the mean thickness of the left side from the black dashed line. Similarly, the average thickness of the vertices $\langle w_v \rangle$ was the mean thickness of the right side of the black dashed line.

2.5.3. Drainage Analysis at the Scale of a Strut

It is interesting to analyze the sample locally, to investigate the drainage at the scale of a strut and to track single strut thicknesses over time or at different foam heights. Local analysis was performed by defining regions of interest (ROIs) with the VG Studio software, to focus on smaller volumes of the sample and carry out specific measurements. In order to track the temporal evolution in a gelling hydrogel foam, a sequence of 15 successive tomograms, each lasting 5 min, was conducted. The total tracking time was 75 min, starting 20 min after the foam fabrication. For each 5 min sequence, a 3D reconstruction was obtained on which four struts were randomly chosen at different locations. A cubic ROI of 0.7 mm width was created to contain the center of a strut (Figure 3b). Using the coordinates of the center of this ROI, this was reproduced on the successive tomograms (at 20, 30, 40, 55, 80, and 90 min in Figure 6c) and for the four struts. As the structure and morphology of the foam changed over time, it was necessary to check that the strut was still contained within the ROI. If this was not the case, the ROI was moved slightly in the x, y, or z direction.

3. Results and Discussion

We focus on LVA-$CaHPO_4$-based systems to highlight the impact of the initial liquid properties (such as the viscosity), the

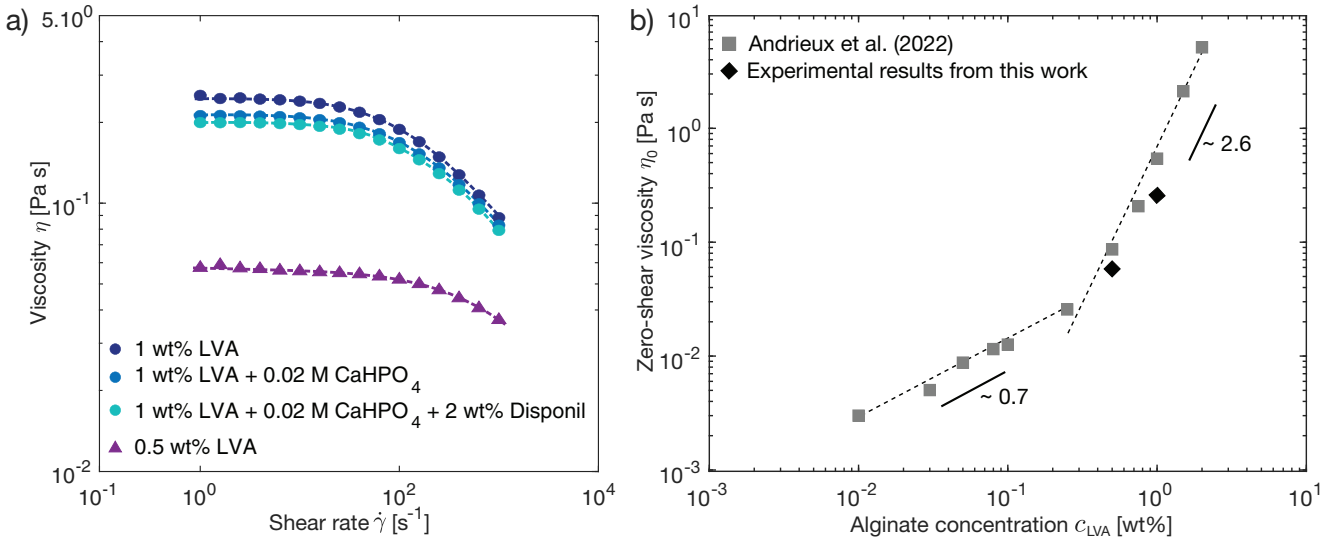

Figure 4. Rheological characterization. a) Viscosity η of different LVA-based solutions as a function of the shear rate $\dot{\gamma}$. The dashed lines correspond to the fit by the Cross model (the obtained fitting parameters are provided in the Supporting Information, Table S1). b) Zero-shear viscosity η_0 of pure LVA solutions as a function of the LVA concentration c_{LVA}. Comparison of our experimental results (for 1 and 0.5 wt% LVA) with S. Andrieux et al. results in grey.[21] The dashed lines are fits to a power law.

gelation kinetics and the drainage, on the morphology of the resulting gelled foam. To do this, we first need to control the initial properties of the foaming liquid, which dictate the initial structure and morphology of the liquid foam when using the bubbling process[17]; and then the solidification kinetics, which has an impact on the foam timescales (drainage) and therefore on the morphology of the solid foam.

3.1. Tuning the Properties of the Initial Foaming Liquid

The variation of the viscosity of different LVA solutions with the shear rate is measured using rheological characterization and is shown in **Figure** 4a for a 1 wt% LVA solution without additives, with 0.02 M $CaHPO_4$ or 0.02 M $CaHPO_4$ + 2 wt% Disponil added to the initial solution, compared to a 0.5 wt% LVA solution without additives. As no GDL is added, there is no gelation. First, we see a decrease in viscosity when $CaHPO_4$ is added. This can be explained by the increase in ions in the presence of the calcium salt, which changes the interactions of the LVA chains.[21,27] The use of the surfactant (Disponil APG 425) does not appear to have a significant effect on viscosity because this surfactant is non-ionic. We notice that all the solutions follow a shear-thinning behavior, which means that the viscosity η decreases as the shear rate $\dot{\gamma}$ increases. This decrease is well captured by the Cross model,[22] which we fit to all the data (the obtained fitting parameters are provided in Table S1, Supporting Information).

We use these fits to obtain the zero-shear viscosity η_0, corresponding to the plateau value of the curves in Figure 4a. Figure 4b compares the zero-shear viscosity of our experimental results with no additives with those from the Andrieux et al.[21] study. We see that the viscosity of LVA solutions increases rapidly with increasing LVA concentration in this concentration range ($\eta_0 \propto c_{LVA}^{2.6}$). Our results are slightly lower than those of Andrieux et al.,[21] which may be due to a change of operator or LVA batch.

These measurements show that the LVA concentration has an important impact on the initial viscosity of the solutions. We will see that this difference in viscosity has indeed an impact on the foam density and on the size of the bubbles produced by bubbling through nozzles (Figure 7a).

3.2. Tuning the Gelation Time

Liquid foams evolve over time, first draining and evaporating, then undergoing coarsening until they break. Working with gelling foams makes it possible to stop these phenomena and controlling solidification allows to "freeze" the foam in a desired intermediate morphology.

Figure 5a shows the evolution of the shear elastic modulus of LVA solutions (c_{LVA} = 1 wt%, 0.02 M $CaHPO_4$ and no surfactant to avoid bubbles) after addition of GDL at different GDL concentrations. We see that gelation is faster at higher GDL concentrations because the shear elastic modulus G' reaches a plateau (called the plateau storage modulus) more quickly at high GDL concentrations. We also notice that the value of this plateau decreases as the GDL concentration increases (Figure 5b). This can be explained by the fact that the gluconate (Gluc) in the GDL chelates calcium ions and competes with LVA, by also bonding to the calcium released by the $CaHPO_4$ particles. Increasing its concentration at a constant LVA concentration leads to an increase in the percentage of Ca–Gluc bonding and therefore a decrease in the percentage of Ca–LVA bonding, which is responsible for the gel's strength at long times.[10] The inset in Figure 5b shows the simulation of the quantity of calcium ions free to cross-link with alginate for different GDL concentrations, using the Hyperquad Simulation and Speciation programme (HySS).[28] We notice that the lower the concentration of GDL in the formulation, the greater the amount of free calcium ions available to create a Ca–LVA bond, consistent with a decrease of the final shear elastic modulus G' of the

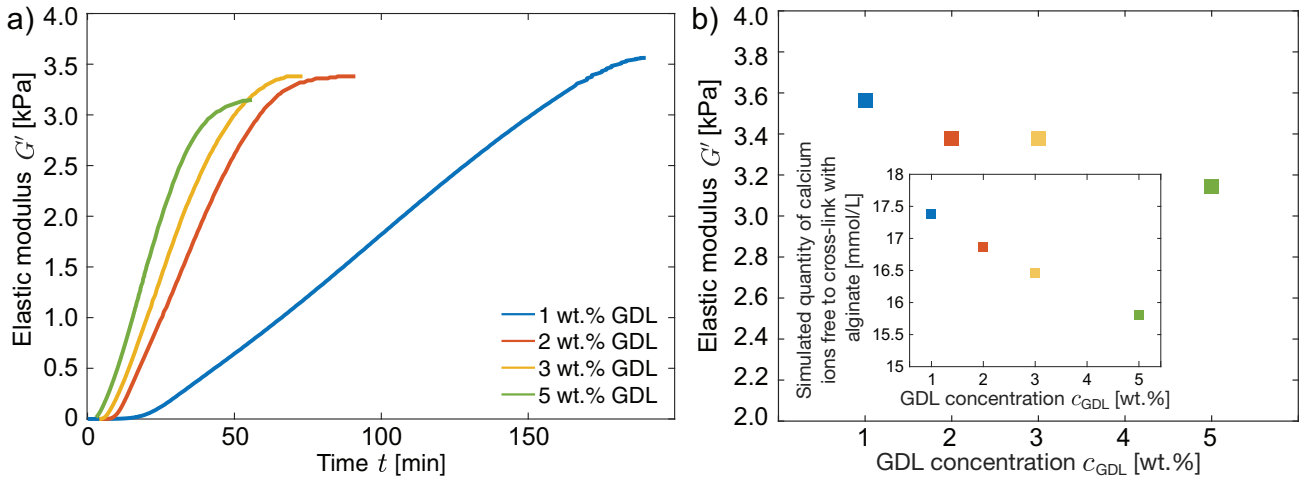

Figure 5. Influence of the GDL concentration on the shear elastic modulus. a) Shear elastic modulus G' as a function of time for LVA solutions (c_{LVA}=1 wt% and 0.02 M $CaHPO_4$, without surfactant) with different GDL concentrations c_{GDL}. b) Plateau moduli G' as a function of c_{GDL} for the formulation presented in (a). Inset: Simulated quantity of calcium ions free to cross-link with alginate (HySS simulation) as a function of c_{GDL}.

samples as a function of c_{GDL}. More details concerning the link between the plateau storage moduli and the amount of calcium ions free to cross-link with alginate for different GDL concentrations are presented in Figure S1 (Supporting Information).

These results show that we can have a real impact on the gelation time by modifying the GDL concentration. We will see that by tuning the gelation time, we can have an impact on the thickness of the foam structure without changing the bubble size, produced by bubbling through nozzles (Figure 7).

3.3. Drainage and Gelation Kinetics

Here, we study drainage both globally over the entire foam (**Figure 6**a,b), and locally over regions of interest containing a strut (Figure 6c,d).

Figure 6a shows the evolution of the drained liquid height, h, as a function of time for different LVA solutions, with and without gelation. All formulations are made with 0.02 M $CaHPO_4$ and 2 wt% of added Disponil, but for ease of reading, we only specify the LVA and GDL concentrations. First, the evolution of the height of the drained liquid h without gelation is shown by the red curve with triangular markers for c_{LVA} = 1 wt%, and the blue curve with circular markers for c_{LVA} = 0.5 wt%. We observe that both formulations attain the same drained liquid plateau height, ≈11 mm, but this plateau is reached more quickly for c_{LVA} = 0.5 wt% than for c_{LVA} = 1 wt%. This can be explained by the fact that the height of the final plateau is fixed by the bubble size and the surface tension,[29] while the time it takes to reach the plateau is controlled by the viscosity of the solution. Since the solution with 0.5 wt% LVA is less viscous, the foam drains more quickly.

Then, the green curves with circular markers represent the results for c_{LVA} = 1 wt% and different GDL concentrations (c_{GDL} = 1, 2, and 3 wt%) leading to gelled foams. We can see a significant difference when the foam is gelled or not. With gelation, the height of the drained liquid plateau is between 6 and 7 mm compared to 11 mm without gelation. We also observe that the higher the concentration of GDL, the faster the plateau height is reached. This can be explained by the fact that solidification is faster with a high concentration of GDL, so the foam drains less and remains in an intermediate state. We expect the foam with more GDL to be denser.

Figure 6c (left axis) shows the evolution of the thickness of four individual struts taken at random positions inside the 3D reconstruction of an LVA foam (c_{LVA} = 1 wt%, 0.02 M $CaHPO_4$, and 2 wt% Disponil and 3 wt% GDL added to the initial solution) at different times. We observe that their thickness decreases with time and seems to stabilize after 30–40 min, which demonstrates that the foams are still draining after 20 min. These observations seem to indicate different drainage time scales in comparison to the results presented in Figure 6a where the foam with c_{LVA} = 1 wt% and c_{GDL} = 3 wt% seems to reach a plateau after only 5 min. We have to consider here the resolution used for the two imaging techniques. In Figure 6c, between 20 and 40 min, we are talking about a decrease in strut thicknesses of ≈50 µm which are not visible by measuring the height of the liquid drained on images taken with the camera resolution used in Figure 6a,b.

The right axis in Figure 6c shows in yellow the shear elastic modulus G' as a function of time for the solution with c_{LVA} = 1 wt% and c_{GDL} = 3 wt%, measured by rheological tests. It seems that the foam drains until the material constituting the foam reaches a stiffness between 2.0 and 3.0 kPa. We can make a clear link between the stop of the evolution of the drainage in the foam and the evolution of the shear elastic modulus as a function of time.

As a side note, in Figure 6c, we observe that the thicknesses of the four struts are not equal. If we consider more closely what is happening inside the foam, we remark that the orientation of these struts is also different (Figure 6d). Indeed, the struts n°3 and 4 are oriented more vertically than the other two, leading to a stronger influence of gravity and hence stronger drainage. The location coordinates of each strut are listed in the Supporting Information (Table S2).

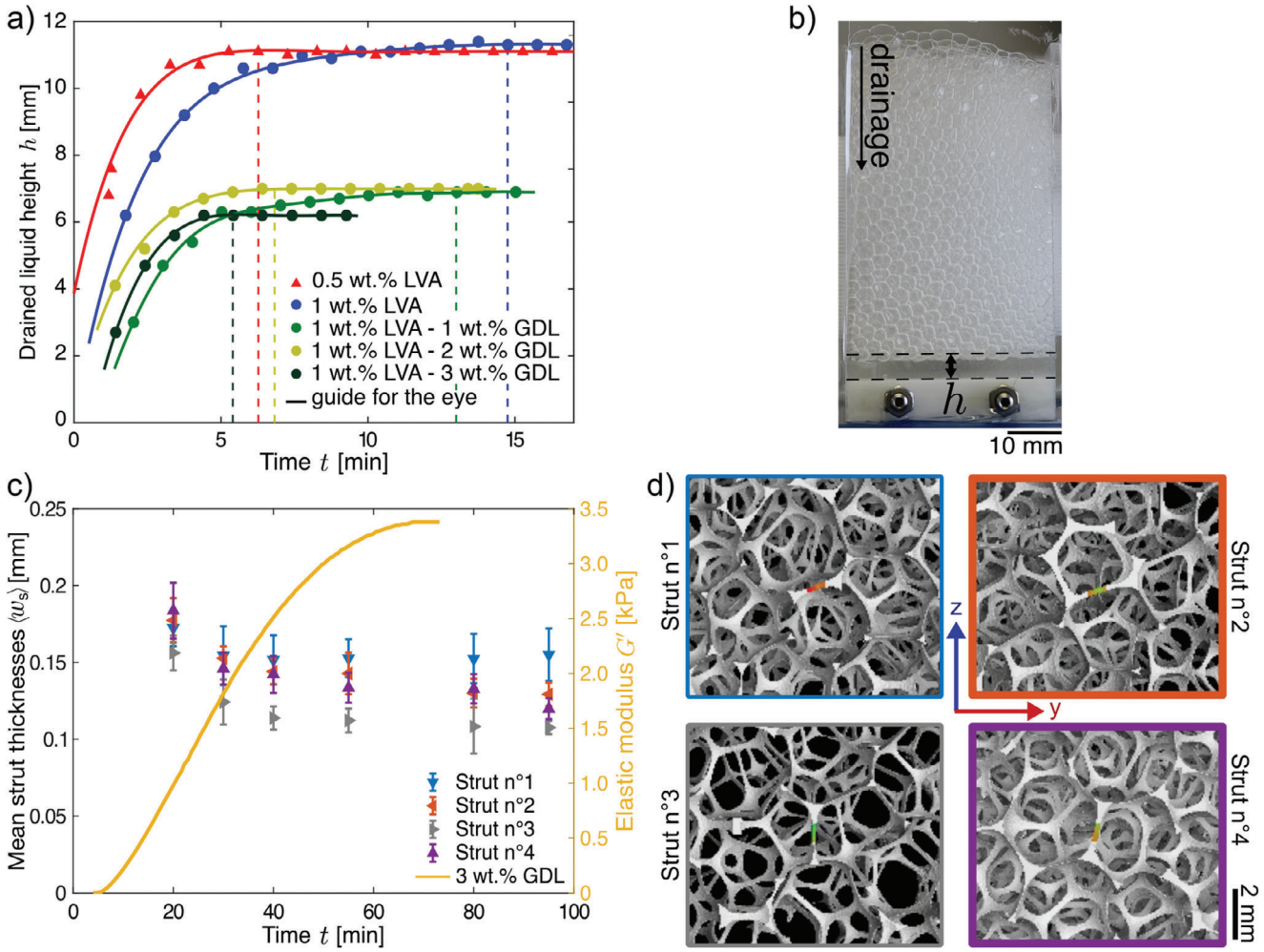

Figure 6. Drainage characterization using an optical camera: a) Drained liquid height h as a function of time t for different LVA solutions (1 or 0.5 wt% LVA, 0.02 M $CaHPO_4$ and 2 wt% of added Disponil) with and without gelation. The GDL concentration is specified in the case of gelation. Dashed lines are a guide for the eye to show, for each formulation, the time at which the height of the drained liquid reaches a plateau. Solid lines are polynomial fits. b) Photograph of the alginate foam on which the drained liquid height h is measured. **Drainage characterization using an optical camera and Drainage characterization using X-ray tomography:** c) Left axis in black: Evolution of the average thickness $\langle w_s \rangle$ of four different struts over time t. The thickness measurements are made with the VG Studio software and focus on the central part of these struts, contained within a 0.7 mm wide cubic ROI (see Figure 3b). The struts were randomly selected from X-ray tomographic images of an LVA foam (1 wt% LVA, 0.02 M $CaHPO_4$, and 2 wt% Disponil and 3 wt% GDL added to the initial solution). The error bars correspond to the standard deviations of the strut thickness. Right axis in yellow: shear elastic modulus G' as a function of time t for the same LVA solution without surfactant. d) Zoom on the four struts reconstructed from tomographic images of the LVA foam. Resolution: 25 µm.

The foam characterizations using a camera or X-ray tomography demonstrate that the GDL concentration controls the solidification kinetics, which stops drainage at a certain point, thus also stopping the evolution of strut and vertex thicknesses. The final shape is thus different from the one obtained for liquid foams at long times.[29] Those profiles depend strongly on the bubble size, and liquid foams with millimetric bubbles usually drain toward liquid fractions smaller than a percent above a height of a few millimeters.

3.4. Control Over the Hydrogel Foam Morphology

With all the results given above concerning the adjustment of the initial liquid properties, gelation time and drainage in relation to the gelation kinetics, we summarize in this section the impact of LVA and GDL concentrations on the resulting LVA foam morphology.

All formulations are made with 0.02 M $CaHPO_4$ and 2 wt% of added Disponil and for ease of reading, we only specify below the LVA and GDL concentrations.

3.4.1. Influence of the Alginate Concentration on the Foam Morphology

Figure 7a shows the foam characteristics (bubble diameters, strut and vertex thickness) measured with the VG Studio software, for two different LVA concentrations (c_{LVA} = 0.75 and 1 wt%, the GDL concentration being kept constant at c_{GDL} = 4 wt%),

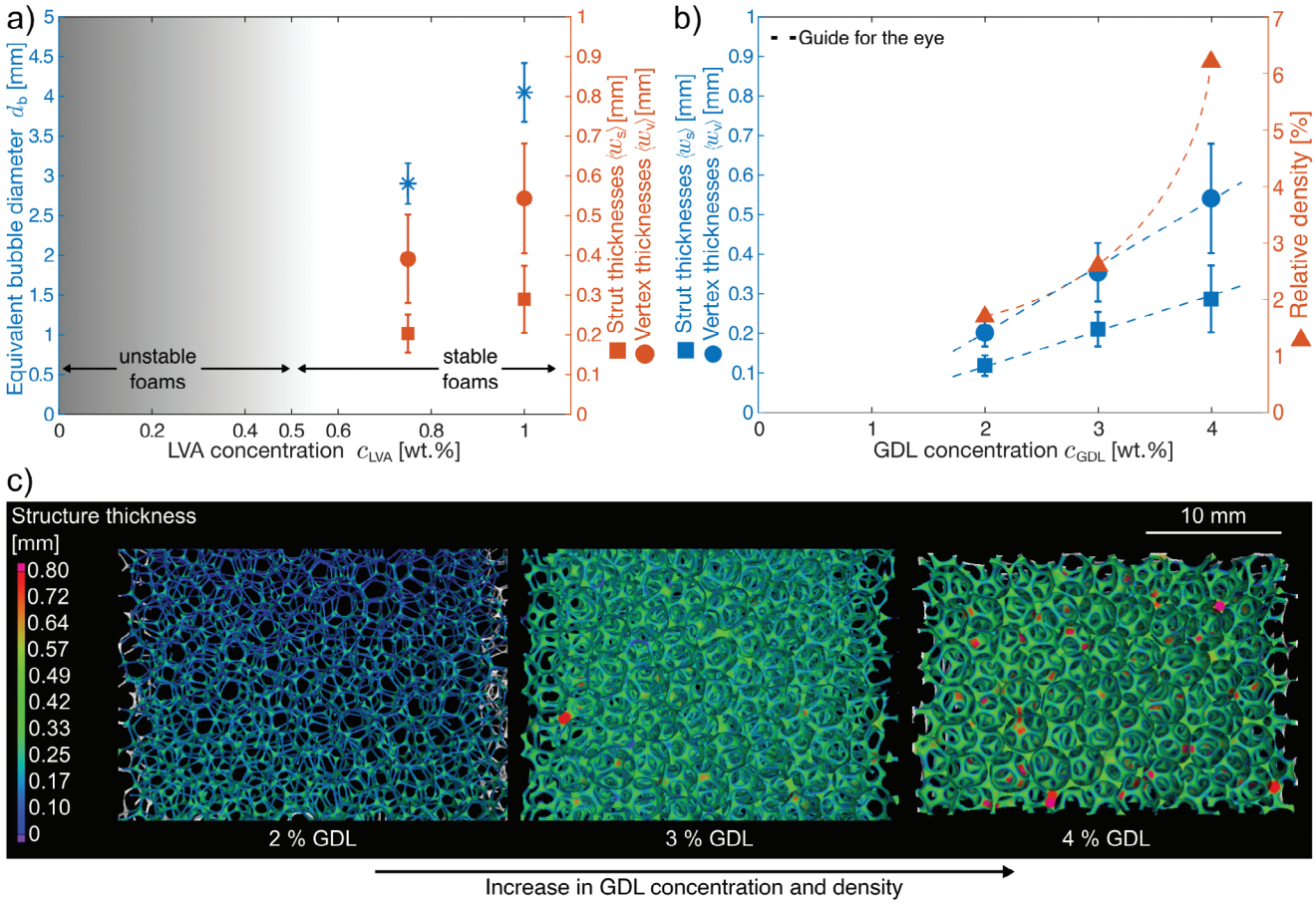

Figure 7. Impact of the formulation on the foam features a) Influence of the LVA concentration: left axis in blue: Equivalent bubble diameters d_b. Right axis in red: Average thickness of struts w_s and vertices w_v over the entire sample. All results are measured with the VG Studio software on LVA foam tomographic scans for different LVA concentrations c_{LVA} (with 0.02 M $CaHPO_4$ + 2 wt% Disponil + 4 wt% GDL). The error bars correspond to standard deviations of bubble diameters or strut thicknesses, respectively, over the entire sample. A foam with c_{LVA} = 0.5 wt% was tested and found to be unstable. 0.5 wt% of LVA is therefore marked on the graph as the boundary between unstable and stable foams. b) Influence of the GDL concentration: left axis in blue: Average thickness of struts $\langle w_s \rangle$ and vertices $\langle w_v \rangle$ over the entire sample. All results are measured with the VG Studio software on LVA foam images for different GDL concentrations c_{GDL} (with c_{LVA} = 1 wt% + 0.02 M $CaHPO_4$ + 2 wt% Disponil). The error bars correspond to the standard deviations of bubble diameters or strut thicknesses, respectively, over the entire sample. Right axis in red: Relative density of the corresponding foam. c) 3D reconstruction of the LVA foams analyzed in Figure 7b. The tomography for the foam with c_{GDL} = 4 wt% is carried out 20 min after the foam fabrication for 20 min. The two other tomographies are carried out 20 min after foam fabrication for 5 min. Resolution: 25 µm.

following the foaming protocol described in the Experimental Section. The tomographic characterizations are carried out 20 min after the foam fabrication with a resolution of 25 µm and for 20 min. First, we can see in Figure 7a (left axis in blue) that the diameter of the bubbles is larger when the solution is more concentrated in LVA. This can be explained by the fact that the viscosity of the solutions increases when the LVA concentration increases (Figure 4a).

Then, Figure 7a (right axis in red) shows the average thicknesses of the struts ($\langle w_s \rangle$) and vertices ($\langle w_v \rangle$). We can see that for both thicknesses, the foam structure is thinner when the LVA concentration is lower. As shown in Section 3.1, this can be explained by the reduction in viscosity, which allows the foam to drain more.

A foam with c_{LVA} = 0.5 wt% and c_{GDL} = 4 wt% was also tested but was found to be unstable because the foam drains too quickly and solidifies too slowly. The various aging mechanisms are then not stopped.

3.4.2. Influence of the GDL Concentration on the Foam Morphology

Figure 7b,c shows the impact of the GDL concentration on the foam characteristics (bubble diameter, strut and vertex thicknesses). Three different GDL concentrations were tested (c_{GDL} = 2, 3, and 4 wt%) at constant LVA concentration (c_{LVA} = 1 wt%). The foam characteristics are measured with the VG Studio software and the foams are produced following the foaming protocol described in the Experimental Section. Tomographic characterization of the LVA foam with 4 wt% GDL is carried out 20 min after foam fabrication with a resolution of 25 µm and for 20 min. Foams containing 2 and 3 wt% GDL are not

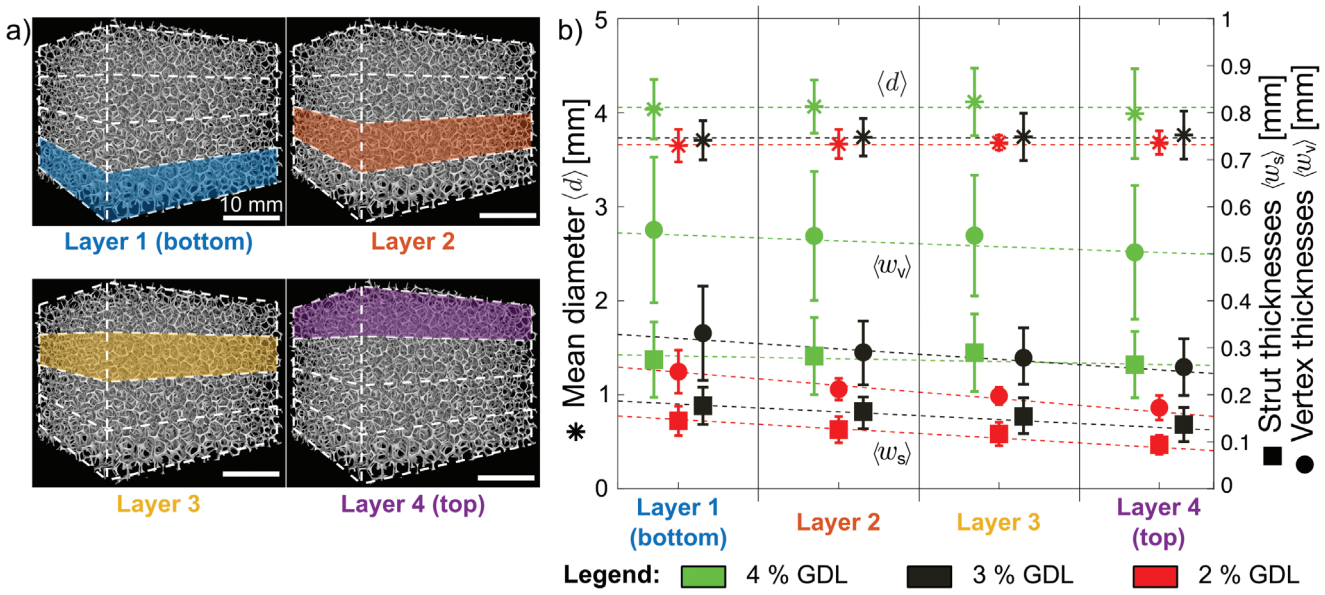

Figure 8. Verification of the sample homogeneity along the *z*-axis. a) Illustration of the layer positions shown on an LVA foam (with c_{LVA} = 1 wt% + 0.02 M $CaHPO_4$ + 2 wt% Disponil and c_{GDL} = 3 wt%) with the corresponding layer highlighted in colour. b) Left axis: Mean diameter of the bubbles (star symbols); Right axis: Mean thicknesses of the struts (square symbols) and vertices (circle symbols) over the corresponding layer, for different GDL concentrations (with c_{LVA} = 1 wt% + 0.02 M $CaHPO_4$ + 2 wt% Disponil). Each point corresponds to the averaged value over the corresponding layer (as illustrated in a)) and the error bars correspond to the standard deviations of the bubble diameter and the structure thicknesses over the corresponding layer. The dashed lines are guides for the eye.

sufficiently stable to be characterized in the same way. Therefore, the results described here, for these two formulations, are taken from the first step of sequential rapid tomography scans described in Section 2.5.3. More specifically, for c_{GDL} = 2 and 3 wt%, the scan is carried out 20 min after foam fabrication at a resolution of 25 µm and for 5 min.

We can see in Figure 7b that the GDL concentration has an impact on the thicknesses of the structure. We observe that both thicknesses (struts and vertices) decrease when the solution is less concentrated in GDL showing that the longer the solidification time, the longer the foam can drain. This is also reflected by the increase in the relative density of the foam as the GDL concentration increases.

3.4.3. Homogeneity of the Samples

To verify the homogeneity of the samples along the *z*-axis, i.e., the sample height, we use the VG Studio software to artificially divide the samples in four layers taken at different *z* positions (**Figure** 8a). We observe in Figure 8b (left axis) that the GDL concentration has no significant impact on the bubble diameters, which vary between 3.6 ± 0.1 and 4 ± 0.4 mm. In terms of the structure thicknesses, there seems to be a thickness gradient in each sample, regardless of the GDL concentration, with struts and vertices at the top of the foam being thinner than those at the bottom, as a result of drainage. However, the difference in thickness between the top and bottom of the foam is smaller for foams with a larger concentration of GDL, which is consistent with a slowing down of the drainage mechanism, as shown in Section 3.4.2.

4. Conclusion

We describe here a method for generating and controlling the morphology of solid foams from liquid foam templates, using the example of Alginate-$CaHPO_4$-based hydrogel foams. The solidification kinetics of such foams can be controlled via the GDL concentration. Using rheological characterization, we show how the formulation, the initial solution viscosity and gelation kinetics influence the foam morphology. We provide a highly controllable foaming process by bubbling nitrogen through nozzles into the solution. We present methods for the characterization of the gelling and gelled foams, which we use to demonstrate that by controlling the initial properties of the liquid (such as the viscosity), solidification kinetics and drainage, we can finely tune the foam morphology (bubble size, structure thickness, homogeneity of the samples). The tomography results show that by decoupling the foam generation and solidification while accounting for foam drainage, it is possible to modify the density of the obtained solid foams. By quantifying the competition between the different timescales involved, the approach described here can be adapted to multiple formulations and length scales of bubble sizes, for systems with a wide variety of purposes, going from model systems that allow a physical understanding of liquid foams frozen in a given state (allowing further structural analysis), to applications in the biomedical field, from scaffolds to wound dressings.

Supporting Information

Supporting Information is available from the Wiley Online Library or from the author.

Acknowledgements

The authors would like to thank Sébastien Andrieux for fruitful discussions and comparison with previously published data (Figure 4), Damien Favier for his help on X-ray microtomography approaches, as well as François Schosseler and Marwan Chammouma for interesting discussions and feedback. All X-ray tomography measurements in this work were performed in the MINAMEC platform of the Institut Charles Sadron. This work of the Interdisciplinary Institute HiFunMat, as part of the ITI 2021-2028 program of the University of Strasbourg, CNRS and Inserm, was supported by IdEx Unistra (ANR-10-IDEX-0002) and SFRI (STRAT'US project, ANR-20-SFRI-0012) under the framework of the French Investments for the Future Program. The authors also acknowledge funding from the IdEx Unistra framework (A. Hourlier-Fargette), the European Research Council (ERC- METAFOAM 819511), and the Agence Nationale de la Recherche (ANR) (FOAMINT project, ANR-23-CE06-0014-01).

Conflict of Interest

The authors declare no conflict of interest.

Data Availability Statement

The data that support the findings of this study are available from the corresponding author upon reasonable request.

Keywords

foams, hydrogels, liquid foam templating, rheology, X-ray tomography

Received: April 19, 2024
Revised: June 27, 2024
Published online:

[1] R. Foudazi, R. Zowada, I. Manas-Zloczower, D. Feke, *Langmuir* **2023**, *39*, 2092.
[2] I. Ben Djemaa, S. Andrieux, S. Auguste, L. Jacomine, M. Tarnowska, W. Drenckhan-Andreatta, *Gels* **2022**, *8*, 444.
[3] C. Stubenrauch, A. Menner, A. Bismarck, W. Drenckhan, *Angew. Chem. Int. Ed.* **2018**, *57*, 10024.
[4] S. Andrieux, A. Quell, C. Stubenrauch, W. Drenckhan, *Adv. Colloid Interface Sci.* **2018**, *256*, 276.
[5] J. Plateau, *Statique Expérimentale et Théorique des Liquides Soumis aux Seules Forces Moléculaires*, Gauthier-Villars, Paris **1873**.
[6] A. Saint-Jalmes, *Soft Matter* **2006**, *2*, 836.
[7] K. Draget, *Handbook of Hydrocolloids: Second Edition*, CRC Press, Boca Raton **2009**, pp. 807–828.
[8] K. Chung, N. Mishra, C. Wang, F. Lin, K. Lin, *Biomicrofluidics* **2009**, *3*, 022403.
[9] X. Liu, L. Qian, T. Shu, Z. Tong, *Polymer* **2003**, *44*, 407.
[10] I. Ben Djemaa, F. Boulmedais, S. Auguste, M. Tarnowska, S. Andrieux, W. Drenckhan-Andreatta, *Langmuir* **2024**, *40*, 10492.
[11] F. Scargiali, A. Busciglio, F. Grisafi, A. Brucato, *Chem. Eng. Techol.* **2014**, *37*, 1507.
[12] W. Drenckhan, A. Saint-Jalmes, *Adv. Colloid Interface Sci.* **2015**, *222*, 228.
[13] E. Kosari, J. Eshrgahi, W. Ahmed, P. Hanafizadeh, *Energy Equip. Sys.* **2019**, *7*, 353.
[14] A. Sattari, P. Hanafizadeh, *Colloids Surf. A: Physicochem. Eng. Asp.* **2019**, *564*, 10.
[15] H. Xiao, S. Geng, A. Chen, C. Yang, F. Gao, T. He, Q. Huang, *Chem. Eng. Sci.* **2019**, *200*, 214.
[16] V. Badam, V. Buwa, F. Durst, *Can. J. Chem. Eng.* **2007**, *85*, 257.
[17] M. Jamialahmadi, M. Zehtaban, H. Müller-Steinhagen, A. Sarrafi, J. Smith, *Trans. IChemE* **2001**, *79A*, 523.
[18] A. Kulkarni, J. Joshi, *Ind. Eng. Chem. Res.* **2005**, *44*, 5873.
[19] I. Ben Djemaa, S. Auguste, W. Drenckhan-Andreatta, S. Andrieux, *Adv. Colloid Interface Sci.* **2021**, *294*, 102478.
[20] C. C. Ruiz, *Sugar-Based Surfactants: Fundamentals and Applications*, CRC Press, Boca Raton **2008**.
[21] S. Andrieux, M. Patil, L. Jacomine, A. Hourlier-Fargette, S. Heitkam, W. Drenckhan, *Macromol. Rapid Commun.* **2022**, *43*, 2200189.
[22] M. Cross, *Rheol. Acta* **1979**, *18*, 608.
[23] H. Winter, F. Chambon, *J. Rheol.* **1986**, *30*, 367.
[24] C. A. Schneider, W. S. Rasband, K. W. Eliceiri, *Nat. Methods* **2012**, *9*, 671.
[25] VGStudio, *Foam/powder analysis module*, https://www.volumegraphics.com/en/products/vgsm/foam-analysis.html.
[26] J. S. Rathore, C. Vienne, Y. Quinsat, C. Tournier, *Weld. World* **2020**, *64*, 1367.
[27] O. Smidsrød, *Carbohydr. Res.* **1969**, *13*, 359.
[28] L. Alderighi, P. Gans, A. Ienco, D. Peters, A. Sabatini, A. Vacca, *Coord. Chem. Rev.* **1999**, *184*, 311.
[29] A. Maestro, W. Drenckhan, E. Rio, R. Höhler, *Soft Matter* **2013**, *9*, 2531.